Research Square

Preprints are preliminary reports that have not undergone peer review.
They should not be considered conclusive, used to inform clinical practice,
or referenced by the media as validated information.

Quantification of Multiple DNA Damage Types in Additive-Free Aqueous Plasmid DNA under Helium Atmospheric-Pressure Plasma Jet Irradiation

Hao Yu

hyu5@nd.edu

University of Notre Dame

Cecilia Julieta Garcia Villavicencio

University of Notre Dame

Sylwia Ptasinska

University of Notre Dame

Research Article

Keywords: Additive-free plasmid DNA, Atmospheric-pressure plasma jet (APPJ), Low-temperature plasma (LTP), Discharge parameters, Reactive oxygen and nitrogen species (RONS), Strand breaks, Base lesions

Posted Date: May 14th, 2026

DOI: https://doi.org/10.21203/rs.3.rs-9645581/v1

License: This work is licensed under a Creative Commons Attribution 4.0 International License.
Read Full License

Additional Declarations: No competing interests reported.

Abstract

Low-temperature plasma (LTP) has attracted increasing attention due to its potential applications in plasma medicine. LTP can modulate the generation of reactive species through plasma–liquid interaction, resulting in modifications of the biomolecular properties of irradiated systems such as DNA. Nevertheless, the quantitative characterization of multiple types of DNA damage and their kinetic responses in additive-free aqueous systems under LTP irradiation remains insufficiently understood. This study systematically examined the effects of a helium atmospheric-pressure plasma jet (APPJ) on multiple types of damage in plasmid DNA. Single-strand breaks (SSBs), double-strand breaks (DSBs), and oxidative base lesions assessed by enzymatic treatment were quantified using gel electrophoresis. With increasing irradiation time, the fraction of undamaged DNA decreased approximately exponentially, suggesting that DNA damage followed a pattern consistent with random radical attacks by plasma-generated species such as hydroxyl radicals (•OH). DNA damage was dominated by strand break formation, while oxidative base lesions were present at relatively lower levels. DSB signals were not detected on the gel, which may be caused by DNA fragmentation following strand break formation, resulting in the loss of detectable bands. Increasing the applied frequency from 1 to 4 kHz increased the SSB yield approximately 2-fold, while increasing the applied voltage from 6 to 12 kV increased the SSB yield approximately 4-fold. Changes in these parameters did not alter the ratio of enzyme-sensitive sites (ESSs) to SSBs, which remained greater than 0 but below unity across all tested conditions, suggesting that the relative distribution of plasma-induced oxidative base damage is independent of the discharge parameters tested.

1. Introduction

Low-temperature plasma (LTP) is a non-equilibrium electric discharge characterized by a high electron temperature relative to the ion temperature and a near-room-temperature gas, enabling high chemical reactivity under ambient conditions[1]. LTP can be generated in dielectric barrier discharge systems, such as atmospheric-pressure plasma jets (APPJs) and plasma needles[2]. In APPJ systems, a gas discharge is generated at atmospheric pressure, and the plasma-produced reactive species are transported by gas flow to the surface of the target[3]. Emitted electrons and excited species formed in the discharge region initiate plasma chemistry with atmospheric vapor, oxygen, and nitrogen, leading to the formation of reactive oxygen and nitrogen species (RONS), which are transported toward the target surface[4]. During the transport of plasma species from the gas phase to the gas–liquid interface and into the bulk liquid, further secondary reactions occur, leading to the formation and accumulation of additional RONS in the aqueous targets [5–10].

Understanding the interactions of plasma reactive species, including RONS, with biomolecular tergets is important for developing plasma medicine applications. Highly reactive RONS can interact with biomolecules, leading to oxidative and nitrosative damage[9, 10]. Among biomolecular targets, DNA serves as the carrier of genetic information, making an understanding of RONS-induced DNA damage

particularly important[11]. In aqueous systems, plasma-generated RONS include hydroxyl radical ($^{\bullet}OH$), ozone (O_3), superoxide anion radical ($O_2^{\bullet-}$), hydrogen peroxide (H_2O_2), nitric oxide (NO), peroxynitrite ($ONOO^-$), nitrite (NO_2^-), and nitrate (NO_3^-)[12]. Among reactive oxygen species, $^{\bullet}OH$ is considered the most reactive species generated by plasma because it can react with DNA molecules at diffusion-limited rates[13]. Although plasma-generated $^{\bullet}OH$ has a short lifetime, it can persist in the aqueous solution through rapid hydrogen-atom exchange reactions with surrounding water molecules[14]. Other oxygen species are generally considered to play limited or indirect roles in DNA damage[8, 15–17]. Singlet oxygen ($^1O_2$) has been reported to selectively oxidize guanine bases[15]. Superoxide anion radicals ($O_2^{\bullet-}$) serve as a precursor to the generation of H_2O_2 or even $^{\bullet}OH$[8]. Although ozone (O_3) has been reported to induce DNA damage, it is primarily present at the gas–liquid interface, which limits its direct oxidative effects in bulk solution[14, 17]. Among reactive nitrogen species (RNS), peroxynitrite-related compounds are considered more important because they can generate $^{\bullet}OH$ through secondary reactions[11, 18]. Other RNS mainly participate in the aqueous-phase chemistry of plasma-generated NO_x, resulting in proton release and a decrease in solution pH[19, 20]. In addition to RONS, plasma also generates other physical agents, such as UV radiation and charged particles (electrons and positive ions), which may also contribute to DNA damage to a lesser extent[11, 14, 21].

Since the first APPJ systems were established, numerous studies have investigated plasma-induced DNA damage in both isolated and cellular DNA[11]. Extensive research has shown that several APPJ parameters, including flow rate, irradiation time, gas composition, and exposure distance, influence the type and yield of DNA damage[21–33]. Previous studies have demonstrated that wet DNA samples are more easily damaged than dry DNA, suggesting that reactive radicals generated in the aqueous phase may play an important role[26]. The addition of reactive oxygen species (ROS) and RNS scavengers increases the fraction of undamaged DNA under identical plasma irradiation conditions, indicating that reactive species such as ONOOH, NO_2^-, NO_3^-, and $^{\bullet}OH$ play a primary role in inducing DNA damage[29]. Similarly, amino acids such as glycine or arginine have been shown to reduce plasma-induced single strand breaks (SSBs) and double strand breaks (DSBs) yields[30]. In contrast, increasing the oxygen or water content in gas flow during He plasma irradiation increases the yield of DNA damage[31]. Likewise, introducing oxygen to the surroundings of a He plasma jet increases the fraction of damaged DNA[23]. Increasing the oxygen percentage in the premixed He/O_2 feed gas also leads to higher SSB and DSB yields and an elevated DSB-to-SSB ratio[32]. Moreover, single-molecule measurements using molecular combing analysis shows that DSB generation rates correlate with APPJ discharge power[33]. Furthermore, cellular studies indicate that plasma irradiation mainly induces SSBs and base lesions, whereas substantial DSB formation is typically associated with gamma-ray irradiation[34]. Nevertheless, other cellular studies demonstrate that DSB formation is also observed under plasma irradiation, depending on the distance and duration of plasma treatment[35].

Despite these established findings, it remains unclear whether multiple types of DNA damage can be quantitatively characterized in an aqueous, additive-free environment, particularly regarding the kinetic response of DNA damage to irradiation time, and how plasma discharge parameters modulate different types of DNA damage. To address these questions, additive-free plasmid DNA was dissolved directly in deionized (DI) water and irradiated with a helium APPJ. DNA damage was quantified by gel electrophoresis to examine its dependence on irradiation time, applied voltage, and frequency. Additionally, enzymatic treatment was employed to convert oxidative base lesions into strand breaks, enabling their detection and quantification.

2. Materials and Methods

2.1 Sample Preparation and Plasma Irradiation

Plasmid DNA (pUC18, 2686 bp) powder was purchased from GenScript USA (Piscataway, NJ, USA). The DNA powder was dissolved directly in DI water as received, and the purity of the DNA solution was confirmed using a NanoDrop spectrophotometer (Thermo Fisher Scientific, Waltham, MA, USA) by measuring the A260/A280 ratio[36]. The DNA solution was then adjusted to a final volume of 80 µL per sample at a concentration of 0.05 µg/µL. It is notable that under scavenger-free conditions, extracted pUC18 DNA has been reported to gradually lose its intact form over a period of weeks, even when stored frozen[37]. Thus, the prepared DNA solution was used promptly to minimize background damage.

The DNA solution was placed in a plastic container and irradiated with a plasma jet. The detailed characteristics of the plasma source were reported previously[36]. Briefly, the APPJ device consisted of two 50-mm-long brass electrodes that served as the powered and grounded electrodes, respectively, separated by 30 mm and mounted outside a fused-silica capillary with an inner diameter of …mm. Ultra-high-purity helium (purity > 99.999%) was introduced into the capillary as the working gas. Helium is commonly used as a working gas for plasma discharges, as it produces large streamer channels, promotes diffuse discharges, and facilitates the formation of more uniform plasma[38]. The plasma was ignited by pulsed high-voltage square signals, and the plasma generated in the region between the electrodes was carried by the gas flow and the electric field out of the capillary, forming a plasma jet several cm long in ambient air. The distance between the fused silica capillary and the sample surface was approximately 2 cm. Plasma irradiation was performed at a flow rate of 2.0 standard liters per minute with treatment durations ranging up to 120 s. Experiments were conducted under ambient laboratory conditions, in which humidity may influence the generation of reactive species such as $^{\bullet}OH$, $^{\bullet}HO_2$, and H_2O_2[39]. Nevertheless, humidity in the surrounding environment has a relatively smaller effect than increasing humidity in the plasma feed gas[31]. The temperature of the plasma jet at the sample surface was approximately 30°C at 6 kV and 1 kHz and remained below 85°C at 10 kV and 4 kHz[40]. Evaporation caused by gas flow and local heating, resulting in a volume loss of approximately 5% of the DNA solution during irradiation, did not affect the quantification. pH changes during irradiation were not

measured directly. As a reference, using the same plasma device, the solution pH of 500 µL of DI water irradiated at 10 kV and 4 kHz for 120 s was reported to decrease to approximately 3.9[41].

2.2 Post-Irradiation Treatment and Gel Electrophoresis

After irradiation, the DNA sample was divided into 4 equal aliquots (approximately 20 µL each), each containing 1 µg of DNA. The 4 aliquots were labeled Control, MOCK, Nth, and Fpg, corresponding to the following treatment groups: untreated DNA; DNA incubated without enzyme (incubation and heating alone); DNA incubated with Nth (endonuclease III); and DNA incubated with Fpg (formamidopyrimidine-DNA glycosylase), respectively. Nth and Fpg were purchased from New England Biolabs (Ipswich, MA, USA). The amounts of Nth and Fpg were set at 2 units per µg of DNA based on preliminary titration experiments and in accordance with the literature[37, 42]. Nth and Fpg were first mixed with their corresponding reaction buffers (10×) to prepare 2 µL enzyme solutions, which were then added to the appropriately labeled tubes and diluted to the recommended concentrations. The Control and MOCK samples were not subjected to enzymatic treatment. Subsequently, MOCK, Nth, and Fpg samples were incubated at 37°C for 30 minutes, while the Control samples were kept at approximately 4°C. During incubation, through its DNA glycosylase activity and associated apurinic/apyrimidinic (AP) lyase activity, Nth removes oxidized pyrimidines (thymine and cytosine), whereas Fpg removes oxidized purines (guanine and adenine), resulting in strand breaks at the damaged sites[43, 44]. After incubation, 3 µL of 0.5 M ethylenediaminetetraacetic acid (EDTA) was added to the Nth- and Fpg-treated samples to terminate the enzymatic reactions.

Electrophoresis was performed on a 0.8% agarose gel prepared by dissolving 240 mg of agarose powder (Bio-Rad, Hercules, CA, USA) in 30 mL of 1× Tris-Borate-EDTA (TBE) buffer (Invitrogen, Carlsbad, CA, USA). Before gel solidification, 3 µL of SYBR Green or SYBR Safe DNA gel stain (Thermo Fisher Scientific) was added to the gel. The DNA sample was mixed with 6× loading dye (Thermo Fisher Scientific), and 200 to 500 ng of DNA was loaded into the gel wells. Within each independent experiment, identical amounts of DNA were loaded across all treatment groups. Differences in DNA loading between experiments do not affect quantification, as the fraction of each DNA form was normalized to the unirradiated control within the same experiment. The gel was placed in the electrophoresis chamber (Bio-Rad) containing 1× TBE buffer. Electrophoresis was conducted at an electric field strength of 7.9 V/cm for 80 minutes, with an applied voltage of 55 V across a 7-cm gel.

2.3 Image Acquisition and Quantification

The gel was imaged after electrophoresis using a Bio-1000F imager (Microtek International Inc., Hsinchu, Taiwan), operated with the accompanying Microtek MiBio Fluo software. Gel images from each independent experiment were acquired using identical exposure times to ensure comparability of DNA band intensities between gels. For quantitative analysis, images recorded at shorter exposure times were selected to ensure that all DNA bands remained within the linear detection range without signal saturation.

Image analysis was performed using ImageJ (NIH, Bethesda, MD, USA), including the Fiji distribution. Quantification was restricted to the three major DNA topological forms and their corresponding gel bands: supercoiled (SC), open circular (OC), and linear (LIN). Minor bands, including denatured and dimer bands, were observed occasionally but showed no consistent dependence on treatment group; they were therefore excluded from quantitative analysis. In addition, fragmented DNA appearing as a diffuse smear was treated as background and excluded from the analysis.

The fraction of each DNA form i (i =SC, OC, or LIN), denoted as F_i, was calculated as follows:

$$F_i = \frac{I_i}{I_0}$$

1

where I_i represents the signal intensity of DNA form i under the given experimental conditions, and I_0 represents the total intensity of the three major DNA bands in the corresponding unirradiated control sample under the same treatment group. Here, cross-sample comparison instead of within-sample comparison was used, because plasma irradiation may degrade part of the DNA into short fragments that are undetectable on the gel, thereby reducing the total detectable DNA amount and distorting the relative fraction of each DNA form. A correction factor of 1.4 was applied to SC band intensities prior to quantitative analysis, because SC-form DNA has been reported to have lower dye-binding efficiency than the other two typological forms[45].

The conversion of SC DNA into other forms indicates the occurrence of strand break events. Since DSB formation requires at least two SSBs in close proximity, DSBs occur at a significantly lower yield than SSBs [46]. Therefore, under the assumption that SC loss reflects random SSB formation, the decay of the fraction of SC DNA (F_{SC}) can be fitted as a function of irradiation time using an exponential decay model based on a Poisson distribution:

$$y = Ae^{-kt}$$

2

Here, *y* is the fraction of SC-form DNA, *A* is the fitted initial amplitude at t = 0, and *t* (s) is irradiation time, *e* is the base of the natural logarithm, and *k* is the decay rate constant describing the SSB formation rate in DNA. Under the assumption that SSB formation occurs randomly, the irradiation time *t* at which y decreases to 0.37 of its initial value, i.e., *y* = 0.37*A*, corresponds to an average of one SSB per DNA molecule. This parameter is defined as t_{37} (s), which is calculated as:

$$t_{37} = 1/k$$

3

The SSB yield, n_{SSB}, representing the rate of SSB formation normalized to the DNA molecular mass (MW_{pUC18}, Da^{1}) per unit irradiation time (s^{1}), was quantified as follows:

$$n_{SSB} = 1/(t_{37} \times MW_{pUC18})$$

4

The molecular weight of pUC18 is 1.75 × 10⁶ Da, based on an average mass of 650 Da per base pair and a total length of 2686 base pairs. For each replicate, n_{SSB} was calculated from the corresponding t_{37} value obtained in that individual experiment, and then the mean n_{SSB} and its associated uncertainty were obtained by averaging over all replicates.

The SSB response index for enzyme-sensitive sites (ESSs), n_{ESS}, was calculated by subtracting the SSB yield of the MOCK group from that of the corresponding enzymatic treatment group, as follows[47]:

$$n_{ESS.x} = n_{Enzyme.x} - n_{MOCK}$$

5

Here, *x* refers to the type of enzymatic treatment (Nth or Fpg). Subsequently, the ESS-to-SSB ratio, $R_{ESS/SSB}$, was calculated as follows:

$$R_{ESS/SSB} = n_{ESS}/n_{SSB}$$

6

Each experiment was performed at least three times independently. Data were analyzed and quantified using Origin (OriginLab, Northampton, MA, USA) and DataGraph (Visual Data Tools, Chapel Hill, NC, USA), and all figures were generated using DataGraph. Data are presented as the mean with its standard deviation.

3. Results and Discussion

Figure 1 shows the fractional changes in the three major DNA forms as a function of irradiation time with discharge paramters of 10 kV and 1 kHz for voltage and frequency, respectively. Fractions of each DNA form were calculated using Eq. 1. Prior to irradiation, the dominant DNA topological form was the SC form, indicating that most of the detectable DNA contained no strand breaks. For the Control and MOCK treatment groups, the fraction of SC-form DNA accounted for more than 90% of the total DNA fraction. In the Nth- and Fpg-treated groups, the SC fraction was lower than in the Control and MOCK groups, and approximately 20% of the OC forms were observed. This difference arises from the enzymatic conversion of pre-existing background base lesions, accumulated during DNA preparation and handling, into detectable strand breaks. With increasing irradiation time, the fraction of SC forms gradually decreased in all treatment groups. Within the same time range, the fraction of the OC forms initially

increased, than reached a plateau, and finally gradually decreased. The fractions of the LIN forms remained relatively low, approximately below 5%, throughout the irradiation period.

Figure 2 shows representative results from a single experiment obtained under plasma irradiation at 10 kV and 1 kHz, highlighting the SC decay behavior and the dynamics of the LIN form across treatment groups. The fraction of SC DNA decreased with increasing irradiation time, following approximately a semi-logarithmic decay. Notably, the LIN form of DNA was reliably detected only in the Fpg-treated samples, in which the fraction of LIN DNA increased at short irradiation times (less than 20 s) and subsequently decreased with prolonged irradiation. In the other treatment conditions (Control, MOCK, and Nth-treated), the LIN fraction remained relatively low and was not clearly distinguishable.

Figure 3 shows the t_{37} (a) and n_{SSB} (b) values for different treatment groups (Control, MOCK, Nth, and Fpg) at an applied frequency of 1 kHz and voltages ranging from 6 to 12 kV. To quantify the observed SC decay and SSB formation rates, t_{37} and n_{SSB} were calculated and compared across treatment groups and discharge parameters. The t_{37} and n_{SSB} values were calculated using Equations 3 and 4, respectively. Under each treatment group, increasing the applied voltage led to a decrease in t_{37} and a corresponding increase in n_{SSB}. Table 1 shows the t_{37} and n_{SSB} values for the Control groups at different voltages and frequencies. The n_{SSB} values in the Control sample at 12 kV were $(18.5 \pm 8.0) \times 10^{-9}$ SSB·Da^{-1}·s^{-1}, 4 times higher than those at 6 kV, which were $(4.7 \pm 1.5) \times 10^{-9}$ SSB·Da^{-1}·s^{-1}. At a given voltage, the MOCK group exhibited t_{37} and n_{SSB} values similar to those of the Control, indicating that incubation and heating alone did not significantly alter DNA topology. In contrast, both Nth- and Fpg-treated groups showed lower t_{37} values relative to the Control, indicating that additional base lesions were successfully detected by enzymatic treatment. No significant difference in t_{37} or n_{SSB} was observed between the Nth- and Fpg-treated groups.

Table 1. The t_{37} values and n_{SSB} values of the Control groups as a function of applied voltage and frequency.

Condition	t_{37} (s)	(10^{-9} SSB·Da^{-1}·s^{-1})
1 kHz, 6 kV	134.2 ± 56.9	4.7 ± 1.5
1 kHz, 8 kV	55.4 ± 19.5	11.3 ± 3.7
1 kHz, 10 kV	44.8 ± 15.0	14.5 ± 6.5
1 kHz, 12 kV	34.3 ± 11.9	18.5 ± 8.0
2 kHz, 10 kV	21.9 ± 4.7	27.0 ± 6.3
4 kHz, 10 kV	21.8 ± 3.4	26.7 ± 3.9

Figure 4 shows the changes in the t_{37} (a) and n_{SSB} (b) values for different treatment groups at a fixed applied voltage of 10 kV and frequencies ranging from 1 to 4 kHz. Increasing the frequency from 1 to 2

kHz led to a noticeable decrease in t_{37} and a corresponding increase in n_{SSB}, while further increasing the frequency to 4 kHz produced only minor additional changes. The n_{SSB} value in the Control group at 4 kHz was (26.7 ± 3.9) × 10^{-9} SSB·Da^{-1}·s^{-1}, almost twice that at 1 kHz, which was (14.5 ± 6.5) × 10^{-9} SSB·Da^{-1}·s^{-1} (Table 1). Similar to the voltage-dependent trends, changes in frequency did not produce significant differences between the MOCK and Control groups, whereas the Nth- and Fpg-treated groups showed lower values than the enzymatically untreated groups, indicating that additional base lesions were successfully detected by the enzymatic treatment. No significant differences in t_{37} or n_{SSB} were observed between the Nth- and Fpg-treated groups.

The ratio of detectable (enzyme-sensitive sites) ESSs to SSBs, $RE_{SS/SSB}$, was used as an evaluation factor for the relative contribution of oxidative base lesions to total DNA damage. It was calculated using Equations 5 and 6 and examined across all irradiation conditions (Figure 5). For all enzymatic treatment groups, was consistently greater than 0 but remained below unity, indicating that ESSs were present but at lower yields than SSBs under all tested conditions. No clear voltage-dependent (Figure 5a) or frequency-dependent (Figure 5b) trends were observed, nor were clear differences found between the Nth- and Fpg-treated groups.

4. Discussion

Based on the presented results, the degradation of the SC DNA form follows a semi-logarithmic dependence on irradiation time (Fig. 2). This suggests that DNA damage, especially SSB formation, induced by plasma reactive species proceeds as a random and independent process, and that the effective probability of strand break formation remains approximately constant throughout the irradiation period in this study. Among RONS, ˙OH is considered the most important factor in DNA damage. Under plasma irradiation, ˙OH can persist in the aqueous phase via the hydrogen-atom exchange reactions [14]. Additionally, during He plasma irradiation, ˙OH-derived products accumulate approximately linearly with irradiation time[48]. Experimental evidence has shown that in the aqueous phase, the SSB yield is proportional to the effective ˙OH yield, and strand break formation follows a random and independent attack model[49]. ˙OH can induce oxidative damage to DNA through double-bond addition, hydrogen abstraction, and electron transfer reactions [50]. Other species, such as H_2O_2, largely generated by recombination of ˙OH, may further contribute to ˙OH formation through secondary reactions, including peroxynitrite-related pathways involving NO_2^- under acidic conditions [12, 18, 19]. In addition, quasi-free electrons in bulk solution were also reported to have the capacity to induce bond cleavage of DNA components via attachment to the N1–C1' glycosidic bond of nucleosides [51].

DSB formation in the Control group did not show significant changes over irradiation time (Fig. 2). However, with increasing irradiation time, the summed intensities of the three major DNA forms (SC/OC/LIN) decreased (See 60 s in Fig. 1). This observation suggests that the DNA was not only transformed among the three major topological forms, but also further degraded into fragments shorter

than the full-lentgh linear form (sub-linear fragments). Indeed, non-major bands, including a band attributed to DNA denaturation[40] and diffuse smear bands, became more apparent with increasing irradiation time in the gel electrophoresis images (not shown here). Previous studies demonstrated that DSB formation requires two independent ·OH attack events, such that the probability of DSB formation is proportional to the square of the probability of SSB formation[46].

ESSs are enzyme-recognizable oxidative base lesions and their associated clustered damage (Figs. 3 and 4). The ratio of ESS-derived strand breaks to the SSB yield, $R_{ESS/SSB}$ (Fig. 5), was used to evaluate their formation level relative to SSB formation. The $R_{ESS/SSB}$ value was consistently less than unity, indicating that oxidative base lesions are generated at a lower yield than SSBs. Previous studies using the same plasmid DNA under nearly identical aqueous conditions but with X-ray irradiation have shown that the yields of Nth- and Fpg-detectable ESSs are almost the same as the yield of prompt SSBs[52]. The difference may be attributed to the different irradiation sources, X-rays and APPJ, as APPJ tends to induce strand breakage and further fragmentation rather than oxidative base lesion formation. No significant difference was observed between the Fpg-sensitive and Nth-sensitive damage yields, which may also be attributed to this reason. Additionally, although the reaction conditions were maintained using a standard 10× buffer, it remains unclear whether plasma-induced long-lived species, such as H_2O_2 or plasma-induced pH changes, may inhibit enzyme activity. Among ESS-derived DSBs, an initial increase followed by a decrease with increasing irradiation time was observed in the Fpg-treated samples, whereas this trend was not detected in the Nth-treated samples (Fig. 2). This selective increase in DSBs suggests the presence of Fpg-sensitive clustered oxidative purine lesions, as the Fpg protein detects oxidized purines such as 8-oxoguanine[53]. Fpg-induced DSBs may arise from clustered oxidative purine lesions or from the conversion of closely spaced SSBs and purine lesions into DSBs. With increasing irradiation time, the DSB signal disappeared, indicating further fragmentation of the LIN form DNA into shorter DNA fragments appearing as a smear in the electrophoresis gel images.

Additionally, changes in plasma discharge parameters, such as frequency and voltage, may influence DNA damage yields by modulating the generation rates of plasma-derived species, including RONS and other reactive species. Higher voltage (Fig. 3) and higher frequency (Fig. 4) resulted in lower t_{37} values, corresponding to an increased DNA damage formation rate, n_{SSB}. However, $R_{ESS/SSB}$ did not show a clear dependence on voltage or frequency. This suggests that changes in frequency and voltage primarily increased the overall DNA damage yield without clearly altering the relative contribution of detectable ESSs to SSBs. Indeed, in plasma irradiation of aqueous solutions, increasing either voltage or frequency, or both, can accelerate the generation rates of ·OH [48, 54, 55], NO_2^- [54, 55], and solvated electrons [56]. However, under constant power in argon plasma, lower frequency combined with higher voltage has been reported to result in higher detectable ·OH yield [55].

Finally, SSB formation was calculated based on the decrease in the undamaged SC form, which can be directly estimated, as it corresponds to the initial topology of plasmid DNA (Figs. 1 and 2). In contrast, DSB formation was estimated from the LIN form, whereas ESSs were assessed indirectly through

incremental SSBs or DSBs generated by enzymatic conversion of the corresponding base lesions, as ESSs (Figs. 3 and 4). Since these estimates for DSBs and enzyme-generated strand breaks do not originate from the initial topology, they are subject to several sources of uncertainty. For DSB estimates, further fragmentation of DSB-containing DNA can generate sub-linear fragmentation that fall outside the three major topological forms, thereby reducing the detectable LIN fraction [57]. For ESS estimates, the detection efficiency may be affected by enzymatic digestion conditions, including enzyme concentration, incubation time, and reaction buffer composition [58].

5. Conclusions

This study systematically investigated helium APPJ-induced DNA damage in aqueous solution. Using additive-free plasmid DNA combined with enzymatic treatment, SSBs, DSBs, and Nth- and Fpg-detectable oxidative base lesions were quantified using gel electrophoresis. With increasing irradiation time, the fraction of undamaged DNA decreased approximately exponentially, suggesting that DNA damage followed a pattern consistent with random attacks by plasma-generated radicals such as $^{\bullet}$OH. DNA damage was dominated by strand break formation, while oxidative base lesions were present at relatively lower levels. Although DSBs were not clearly detected, the fraction of non-major bands increased, indicating that DNA further degraded into sub-linear fragments that fall outside the three major topological forms. Fpg-treated samples showed increased DSB formation, suggesting the possible presence of Fpg-sensitive clustered oxidative purine lesions. Increasing the applied voltage and frequency decreased the time required to produce the same level of SSB damage (t_{37}), corresponding to an increased SSB formation rate per unit time (n_{SSB}). These results may be attributed to the higher RONS generation rates modulated by changes in discharge parameters. However, changes in voltage and frequency did not significantly affect $R_{ESS/SSB}$, indicating that plasma parameters mainly alter RONS production rates rather than the relative contribution of ESSs to SSBs within the tested ranges. These results provide insight into plasma-induced DNA damage mechanisms and may contribute to the advancement of plasma medicine applications.

Declarations

Acknowledgment

This project was supported by the U.S. Department of Energy, Office of Science, Office of Basic Energy Sciences under Award No. DE-FC02-04ER15533. This work is a contribution number NDRL 5505 from the Notre Dame Radiation Laboratory.

The authors used ChatGPT (OpenAI) and Claude (Anthropic) to assist with language editing and proofreading. All scientific content, data interpretation, and conclusions are the responsibility of the authors.

Data Availability Statement

The authors confirm that the data supporting this study's findings are available within the article and its supplementary materials.

Author Contribution Statement

CRediT roles:

- Hao Yu: Conceptualization, Investigation, Formal analysis, Visualization, Writing – Original draft, Writing – Review and editing
- Cecilia Julieta Garcia Villavicencio: Investigation, Data curation, Writing – Review and editing
- Sylwia Ptasińska: Supervision, Funding acquisition, Writing – Review and editing

References

1. Fridman, G.; Friedman, G.; Gutsol, A.; Shekhter, A. B.; Vasilets, V. N.; Fridman, A. Applied plasma medicine. *Plasma Processes and Polymers* **2008**, *5* (6), 503–533. DOI: 10.1002/ppap.200700154.
2. Hoffmann, C.; Berganza, C.; Zhang, J. Cold Atmospheric Plasma: methods of production and application in dentistry and oncology. *Med Gas Res* **2013**, *3* (1), 21. DOI: 10.1186/2045-9912-3-21.
3. Schütze, A.; Jeong, J. Y.; Babayan, S. E.; Park, J.; Selwyn, G. S.; Hicks, R. F. The atmospheric-pressure plasma jet: A review and comparison to other plasma sources. *Ieee Transactions on Plasma Science* **1998**, *26* (6), 1685–1694. DOI: 10.1109/27.747887.
4. Norberg, S. A.; Johnsen, E.; Kushner, M. J. Formation of reactive oxygen and nitrogen species by repetitive negatively pulsed helium atmospheric pressure plasma jets propagating into humid air. *Plasma Sources Sci T* **2015**, *24* (3), 035026. DOI: 10.1088/0963-0252/24/3/035026.
5. Bruggeman, P.; Leys, C. Non-thermal plasmas in and in contact with liquids. *J Phys D Appl Phys* **2009**, *42* (5), 053001. DOI: 10.1088/0022-3727/42/5/053001.
6. Samukawa, S.; Hori, M.; Rauf, S.; Tachibana, K.; Bruggeman, P.; Kroesen, G.; Whitehead, J. C.; Murphy, A. B.; Gutsol, A. F.; Starikovskaia, S.; et al. The 2012 Plasma Roadmap. *J Phys D Appl Phys* **2012**, *45* (25), 253001. DOI: 10.1088/0022-3727/45/25/253001.
7. Khlyustova, A.; Labay, C.; Machala, Z.; Ginebra, M.-P.; Canal, C. Important parameters in plasma jets for the production of RONS in liquids for plasma medicine: A brief review. *Frontiers of Chemical Science and Engineering* **2019**, *13* (2), 238–252. DOI: 10.1007/s11705-019-1801-8.
8. Graves, D. B. Low temperature plasma biomedicine: A tutorial reviewa). *Physics of Plasmas* **2014**, *21* (8), 080901. DOI: 10.1063/1.4892534.
9. Graves, D. B. The emerging role of reactive oxygen and nitrogen species in redox biology and some implications for plasma applications to medicine and biology. *J Phys D Appl Phys* **2012**, *45* (26), 263001. DOI: 10.1088/0022-3727/45/26/263001.
10. Graves, D. B. Reactive Species from Cold Atmospheric Plasma: Implications for Cancer Therapy. *Plasma Processes and Polymers* **2014**, *11* (12), 1120–1127. DOI: 10.1002/ppap.201400068.

11. Arjunan, K. P.; Sharma, V. K.; Ptasinska, S. Effects of atmospheric pressure plasmas on isolated and cellular DNA-a review. *Int J Mol Sci* **2015**, *16* (2), 2971–3016. DOI: 10.3390/ijms16022971.
12. KC, S. K.; Ghimire, B.; Hong, S.-H.; Oh, J.-S.; Szili, E. J. How to control the plasma jet production of reactive species for medical therapy? A topical review. *Journal of Physics D: Applied Physics* **2025**. DOI: 10.1088/1361-6463/adb316.
13. Buxton, G. V.; Greenstock, C. L.; Helman, W. P.; Ross, A. B. Critical Review of rate constants for reactions of hydrated electrons, hydrogen atoms and hydroxyl radicals (·OH/·O− in Aqueous Solution. *Journal of Physical and Chemical Reference Data* **1988**, *17* (2), 513–886. DOI: 10.1063/1.555805.
14. Bruggeman, P. J.; Kushner, M. J.; Locke, B. R.; Gardeniers, J. G. E.; Graham, W. G.; Graves, D. B.; Hofman-Caris, R. C. H. M.; Maric, D.; Reid, J. P.; Ceriani, E.; et al. Plasma-liquid interactions: a review and roadmap. *Plasma Sources Sci T* **2016**, *25* (5), 053002. DOI: 10.1088/0963-0252/25/5/053002.
15. Pratviel, G.; Meunier, B. Guanine Oxidation: One- and Two-Electron Reactions. *Chemistry – A European Journal* **2006**, *12* (23), 6018–6030. DOI: 10.1002/chem.200600539.
16. Andrés, C. M. C.; Pérez de la Lastra, J. M.; Andrés Juan, C.; Plou, F. J.; Pérez-Lebeña, E. Superoxide Anion Chemistry-Its Role at the Core of the Innate Immunity. *Int J Mol Sci* **2023**, *24* (3). DOI: 10.3390/ijms24031841.
17. Ito, K.; Inoue, S.; Hiraku, Y.; Kawanishi, S. Mechanism of site-specific DNA damage induced by ozone. *Mutation Research/Genetic Toxicology and Environmental Mutagenesis* **2005**, *585* (1), 60–70. DOI: 10.1016/j.mrgentox.2005.04.004.
18. Szabo, C.; Ischiropoulos, H.; Radi, R. Peroxynitrite: biochemistry, pathophysiology and development of therapeutics. *Nat Rev Drug Discov* **2007**, *6* (8), 662–680. DOI: 10.1038/nrd2222.
19. Lukes, P.; Dolezalova, E.; Sisrova, I.; Clupek, M. Aqueous-phase chemistry and bactericidal effects from an air discharge plasma in contact with water: evidence for the formation of peroxynitrite through a pseudo-second-order post-discharge reaction of H2O2and HNO2. *Plasma Sources Science and Technology* **2014**, *23* (1), 015019. DOI: 10.1088/0963-0252/23/1/015019.
20. Machala, Z.; Tarabova, B.; Hensel, K.; Spetlikova, E.; Sikurova, L.; Lukes, P. Formation of ROS and RNS in Water Electro-Sprayed through Transient Spark Discharge in Air and their Bactericidal Effects. *Plasma Processes and Polymers* **2013**, *10* (7), 649–659. DOI: 10.1002/ppap.201200113.
21. Ptasinska, S.; Bahnev, B.; Stypczynska, A.; Bowden, M.; Mason, N. J.; Braithwaite, N. S. DNA strand scission induced by a non-thermal atmospheric pressure plasma jet. *Phys Chem Chem Phys* **2010**, *12* (28), 7779–7781. DOI: 10.1039/c001188f.
22. Yan, X.; Zou, F.; Lu, X. P.; He, G. Y.; Shi, M. J.; Xiong, Q.; Gao, X.; Xiong, Z. L.; Li, Y.; Ma, F. Y.; et al. Effect of the atmospheric pressure nonequilibrium plasmas on the conformational changes of plasmid DNA. *Applied Physics Letters* **2009**, *95* (8). DOI: 10.1063/1.3212739.
23. Young Kim, J.; Lee, D.-H.; Ballato, J.; Cao, W.; Kim, S.-O. Reactive oxygen species controllable non-thermal helium plasmas for evaluation of plasmid DNA strand breaks. *Applied Physics Letters* **2012**, *101* (22). DOI: 10.1063/1.4768922.

24. Han, X.; Cantrell, W. A.; Escobar, E. E.; Ptasinska, S. Plasmid DNA damage induced by helium atmospheric pressure plasma jet. *European Physical Journal D* **2014**, *68* (3), 46. DOI: 10.1140/epjd/e2014-40753-y.
25. Alkawareek, M. Y.; Gorman, S. P.; Graham, W. G.; Gilmore, B. F. Potential cellular targets and antibacterial efficacy of atmospheric pressure non-thermal plasma. *Int J Antimicrob Agents* **2014**, *43* (2), 154–160. DOI: 10.1016/j.ijantimicag.2013.08.022.
26. Yaopromsiri, C.; Yu, L. D.; Sarapirom, S.; Thopan, P.; Boonyawan, D. Effect of cold atmospheric pressure He-plasma jet on DNA change and mutation. *Nuclear Instruments & Methods in Physics Research Section B-Beam Interactions with Materials and Atoms* **2015**, *365*, 399–403. DOI: 10.1016/j.nimb.2015.07.100.
27. Adhikari, E. R.; Ptasinska, S. Correlation between helium atmospheric pressure plasma jet (APPJ) variables and plasma induced DNA damage. *The European Physical Journal D* **2016**, *70* (9), 180.
28. Das, S.; Gajula, V. P.; Mohapatra, S.; Singh, G.; Kar, S. Role of cold atmospheric plasma in microbial inactivation and the factors affecting its efficacy. *Health Sciences Review* **2022**, *4*, 100037. DOI: 10.1016/j.hsr.2022.100037.
29. Kyzek, S.; Pistekova, S.; Kyzekova, I.; Sevcovicova, A.; Kovacik, D.; Zahoranova, A.; Galova, E. Identification of Plasma-Generated Reactive Species in Water and Their DNA-Damaging Effects on Plasmid and Lymphocyte DNA. *Int J Mol Sci* **2025**, *26* (19), 9385. DOI: 10.3390/ijms26199385.
30. Stypczyńska, A.; Ptasińska, S.; Bahnev, B.; Bowden, M.; Braithwaite, N. S. J.; Mason, N. J. The influence of amino acids on DNA damage induced by cold plasma radiation. *Chemical Physics Letters* **2010**, *500* (4-6), 313–317.
31. Adhikari, E. R.; Samara, V.; Ptasinska, S. Influence of O2or H2O in a plasma jet and its environment on plasma electrical and biochemical performances. *Journal of Physics D: Applied Physics* **2018**, *51* (18), 185202. DOI: 10.1088/1361-6463/aab8f0.
32. Alkawareek, M. Y.; Alshraiedeh, N. a. H.; Higginbotham, S.; Flynn, P. B.; Algwari, Q. T.; Gorman, S. P.; Graham, W. G.; Gilmore, B. F. Plasmid DNA Damage Following Exposure to Atmospheric Pressure Nonthermal Plasma: Kinetics and Influence of Oxygen Admixture. **2014**, *4* (1-4), 211–219. DOI: 10.1615/PlasmaMed.2015011977.
33. Kurita, H.; Nakajima, T.; Yasuda, H.; Takashima, K.; Mizuno, A.; Wilson, J. I. B.; Cunningham, S. Single-molecule measurement of strand breaks on large DNA induced by atmospheric pressure plasma jet. *Applied Physics Letters* **2011**, *99* (19). DOI: Artn 19150410.1063/1.3660581.
34. Lazović, S.; Maletić, D.; Leskovac, A.; Filipović, J.; Puač, N.; Malović, G.; Joksić, G.; Petrović, Z. L. Plasma induced DNA damage: Comparison with the effects of ionizing radiation. *Applied Physics Letters* **2014**, *105* (12). DOI: 10.1063/1.4896626.
35. Han, X.; Klas, M.; Liu, Y.; Sharon Stack, M.; Ptasinska, S. DNA damage in oral cancer cells induced by nitrogen atmospheric pressure plasma jets. *Applied Physics Letters* **2013**, *102* (23). DOI: 10.1063/1.4809830.

36. Adhikari, E. R.; Ptasinska, S. Correlation between helium atmospheric pressure plasma jet (APPJ) variables and plasma induced DNA damage. *European Physical Journal D* **2016**, *70* (9), 180. DOI: 10.1140/epjd/e2016-70274-6.
37. Yu, H.; Kondo, Y.; Fujii, K.; Yokoya, A.; Yamashita, S. Establishment of a Method for Investigating Direct and Indirect Actions of Ionizing Radiation Using Scavenger-free Plasmid DNA. *Radiat Res* **2022**, *197* (6), 594–604. DOI: 10.1667/RADE-21-00057.1.
38. Kogelschatz, U. Dielectric-barrier discharges: Their history, discharge physics, and industrial applications. *Plasma Chemistry and Plasma Processing* **2003**, *23* (1), 1–46. DOI: 10.1023/A:1022470901385.
39. Gaens, W. V.; Bogaerts, A. Kinetic modelling for an atmospheric pressure argon plasma jet in humid air. *Journal of Physics D: Applied Physics* **2013**, *46* (27), 275201. DOI: 10.1088/0022-3727/46/27/275201.
40. Sebastian, A.; Lipa, D.; Ptasinska, S. DNA Strand Breaks and Denaturation as Probes of Chemical Reactivity versus Thermal Effects of Atmospheric Pressure Plasma Jets. *ACS Omega* **2023**, *8* (1), 1663–1670. DOI: 10.1021/acsomega.2c07262.
41. Villavicencio, C. J. G.; Silva, B. d. C.; Matara, A.; Ptasinska, S. Exploring pH Dynamics in Amino Acid Solutions Under Low-Temperature Plasma Exposure. *Molecules* **2024**, *29* (24), 5889.
42. Tsao, D.; Kalogerinis, P.; Tabrizi, I.; Dingfelder, M.; Stewart, R. D.; Georgakilas, A. G. Induction and Processing of Oxidative Clustered DNA Lesions in 56Fe-Ion-Irradiated Human Monocytes. *Radiation Research* **2007**, *168* (1), 87–97. DOI: 10.1667/rr0865.1.
43. Dizdaroglu, M.; Laval, J.; Boiteux, S. Substrate specificity of the Escherichia coli endonuclease III: excision of thymine-and cytosine-derived lesions in DNA produced by radiation-generated free radicals. *Biochemistry* **1993**, *32* (45), 12105–12111.
44. Tchou, J.; Bodepudi, V.; Shibutani, S.; Antoshechkin, I.; Miller, J.; Grollman, A. P.; Johnson, F. Substrate specificity of Fpg protein. Recognition and cleavage of oxidatively damaged DNA. *Journal of Biological Chemistry* **1994**, *269* (21), 15318–15324. DOI: 10.1016/S0021-9258(17)36608-5.
45. Milligan, J. R.; Arnold, A. D.; Ward, J. F. The effect of superhelical density on the yield of single-strand breaks in gamma-irradiated plasmid DNA. *Radiat Res* **1992**, *132* (1), 69–73.
46. Milligan, J. R.; Aguilera, J. A.; Nguyen, T. T.; Paglinawan, R. A.; Ward, J. F. DNA strand-break yields after post-irradiation incubation with base excision repair endonucleases implicate hydroxyl radical pairs in double-strand break formation. *Int J Radiat Biol* **2000**, *76* (11), 1475–1483. DOI: 10.1080/09553000050176234 From NLM Medline.
47. Shiraishi, I.; Shikazono, N.; Suzuki, M.; Fujii, K.; Yokoya, A. Efficiency of radiation-induced base lesion excision and the order of enzymatic treatment. *International Journal of Radiation Biology* **2017**, *93* (3), 295–302. DOI: 10.1080/09553002.2017.1239849.
48. Ducrozet, F.; Sebastian, A.; Villavicencio, C. J. G.; Ptasinska, S.; Sicard-Roselli, C. Quantifying hydroxyl radicals generated by a low-temperature plasma using coumarin: methodology and precautions. *Physical Chemistry Chemical Physics* **2024**, *26* (11), 8651–8657. DOI: 10.1039/d4cp00040d.

49. Milligan, J. R.; Ward, J. F. Yield of single-strand breaks due to attack on DNA by scavenger-derived radicals. *Radiat Res* **1994**, *137* (3), 295–299.
50. von Sonntag, C. *Free-radical-induced DNA damage and its repair*; Springer, 2006.
51. Ma, J.; Kumar, A.; Muroya, Y.; Yamashita, S.; Sakurai, T.; Denisov, S. A.; Sevilla, M. D.; Adhikary, A.; Seki, S.; Mostafavi, M. Observation of dissociative quasi-free electron attachment to nucleoside via excited anion radical in solution. *Nat Commun* **2019**, *10* (1), 102. DOI: 10.1038/s41467-018-08005-z.
52. Shiina, T.; Watanabe, R.; Shiraishi, I.; Suzuki, M.; Sugaya, Y.; Fujii, K.; Yokoya, A. Induction of DNA damage, including abasic sites, in plasmid DNA by carbon ion and X-ray irradiation. *Radiation and Environmental Biophysics* **2013**, *52* (1), 99–112. DOI: 10.1007/s00411-012-0447-4.
53. Tchou, J.; Kasai, H.; Shibutani, S.; Chung, M. H.; Laval, J.; Grollman, A. P.; Nishimura, S. 8-oxoguanine (8-hydroxyguanine) DNA glycosylase and its substrate specificity. *Proceedings of the National Academy of Sciences* **1991**, *88* (11), 4690–4694. DOI: 10.1073/pnas.88.11.4690.
54. Baek, E. J.; Joh, H. M.; Kim, S. J.; Chung, T. H. Effects of the electrical parameters and gas flow rate on the generation of reactive species in liquids exposed to atmospheric pressure plasma jets. *Physics of Plasmas* **2016**, *23* (7). DOI: 10.1063/1.4959174.
55. Liu, K.; Xia, H.; Yang, M.; Geng, W.; Zuo, J.; Ostrikov, K. Insights into generation of OH radicals in plasma jets with constant power: The effects of driving voltage and frequency. *Vacuum* **2022**, *198*, 110901. DOI: 10.1016/j.vacuum.2022.110901.
56. Sebastian, A.; Ducrozet, F.; Sicard-Roselli, C.; Ptasinska, S. Assessing solvated electron uptake in low-temperature plasma-exposed solutions as a pathway to quantifying plasma electrons. *The Journal of Chemical Physics* **2024**, *161* (20).
57. Leloup, C.; Garty, G.; Assaf, G.; Cristovão, A.; Breskin, A.; Chechik, R.; Shchemelinin, S.; Paz-Elizur, T.; Livneh, Z.; Schulte, R. W.; et al. Evaluation of lesion clustering in irradiated plasmid DNA. *International Journal of Radiation Biology* **2005**, *81* (1), 41–54. DOI: 10.1080/09553000400017895.
58. Gulston, M.; Fulford, J.; Jenner, T.; de Lara, C.; O'Neill, P. Clustered DNA damage induced by gamma radiation in human fibroblasts (HF19), hamster (V79-4) cells and plasmid DNA is revealed as Fpg and Nth sensitive sites. *Nucleic Acids Res* **2002**, *30* (15), 3464–3472. DOI: 10.1093/nar/gkf467 Medline.

Figures

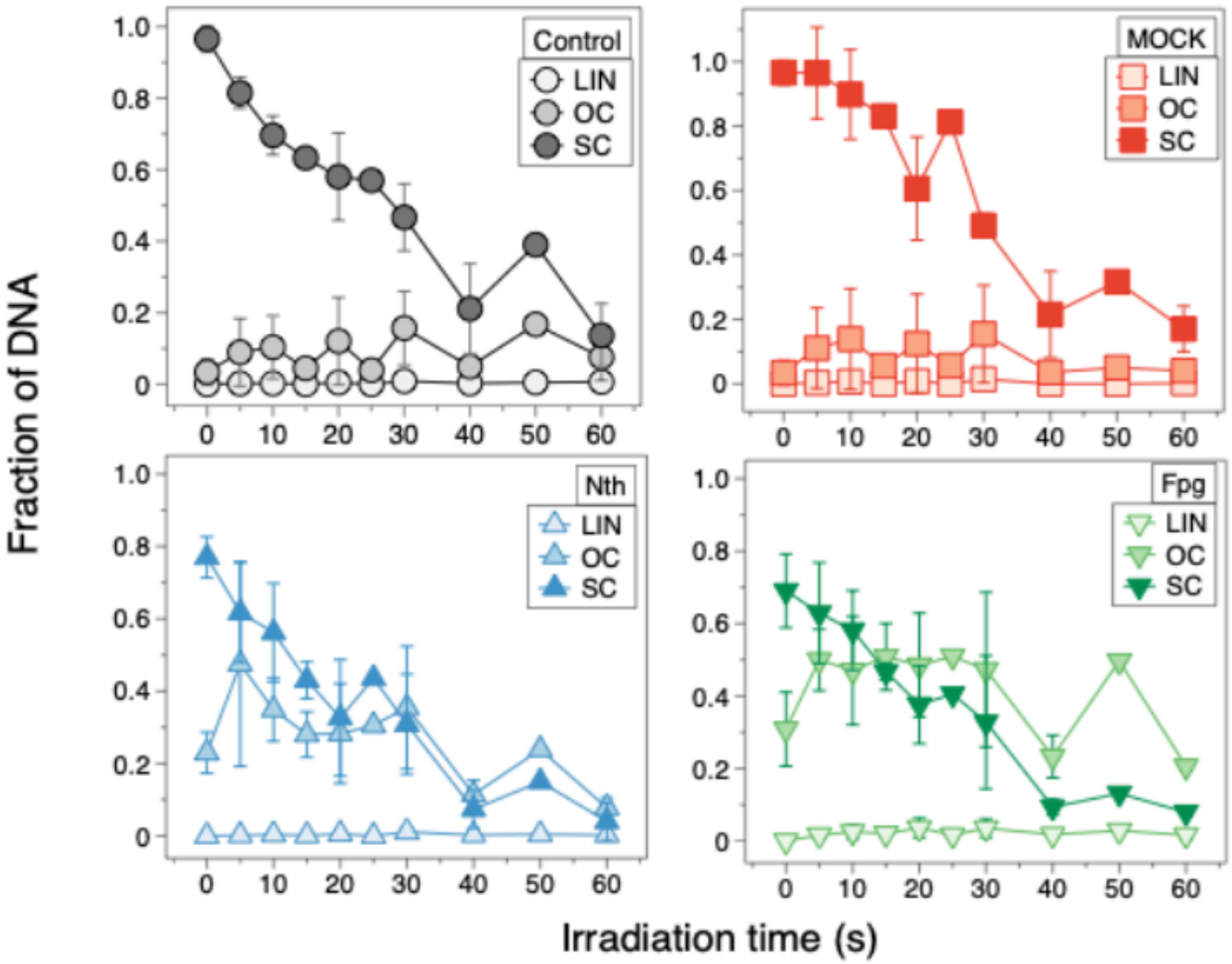

Figure 1

Changes in the fraction of plasmid DNA topological forms (SC, OC, and LIN) in Control, MOCK, Nth-, and Fpg-treated groups under plasma irradiation at 10 kV and 1 kHz. Error bars represent the standard deviation of repeated independent experiments. The dashed line corresponds to the SC form and is provided as a guide to the eye.

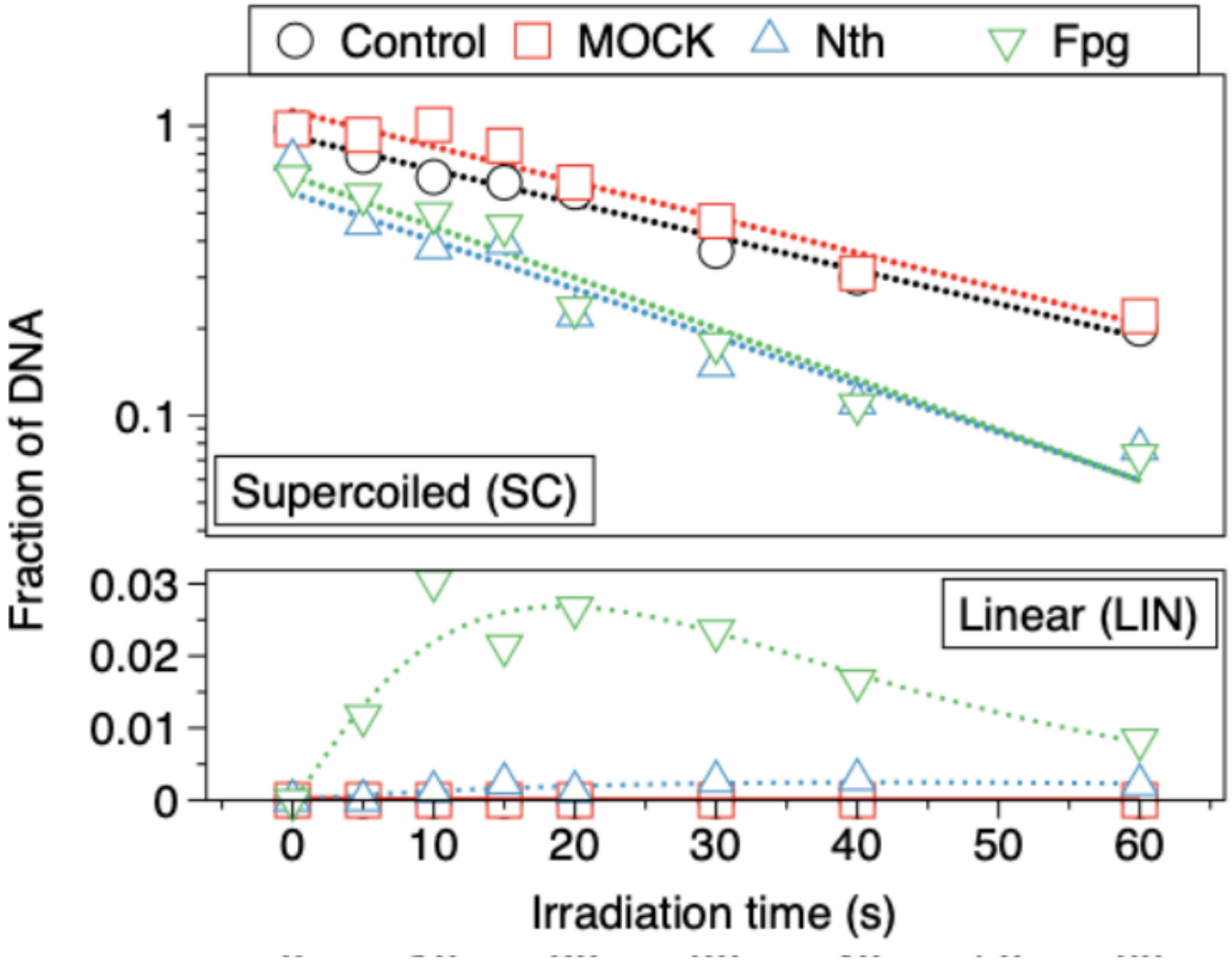

Figure 2

Changes in the fraction of two plasmid DNA topological forms: supercoiled (SC) and linear (LIN) forms as a function of irradiation time in aqueous solution under 10 kV, 1 kHz plasma irradiation. The dashed line for the SC form represents a fitted curve displayed on a semi-logarithmic scale, and the dashed line for the LIN form is provided as a guide to the eye.

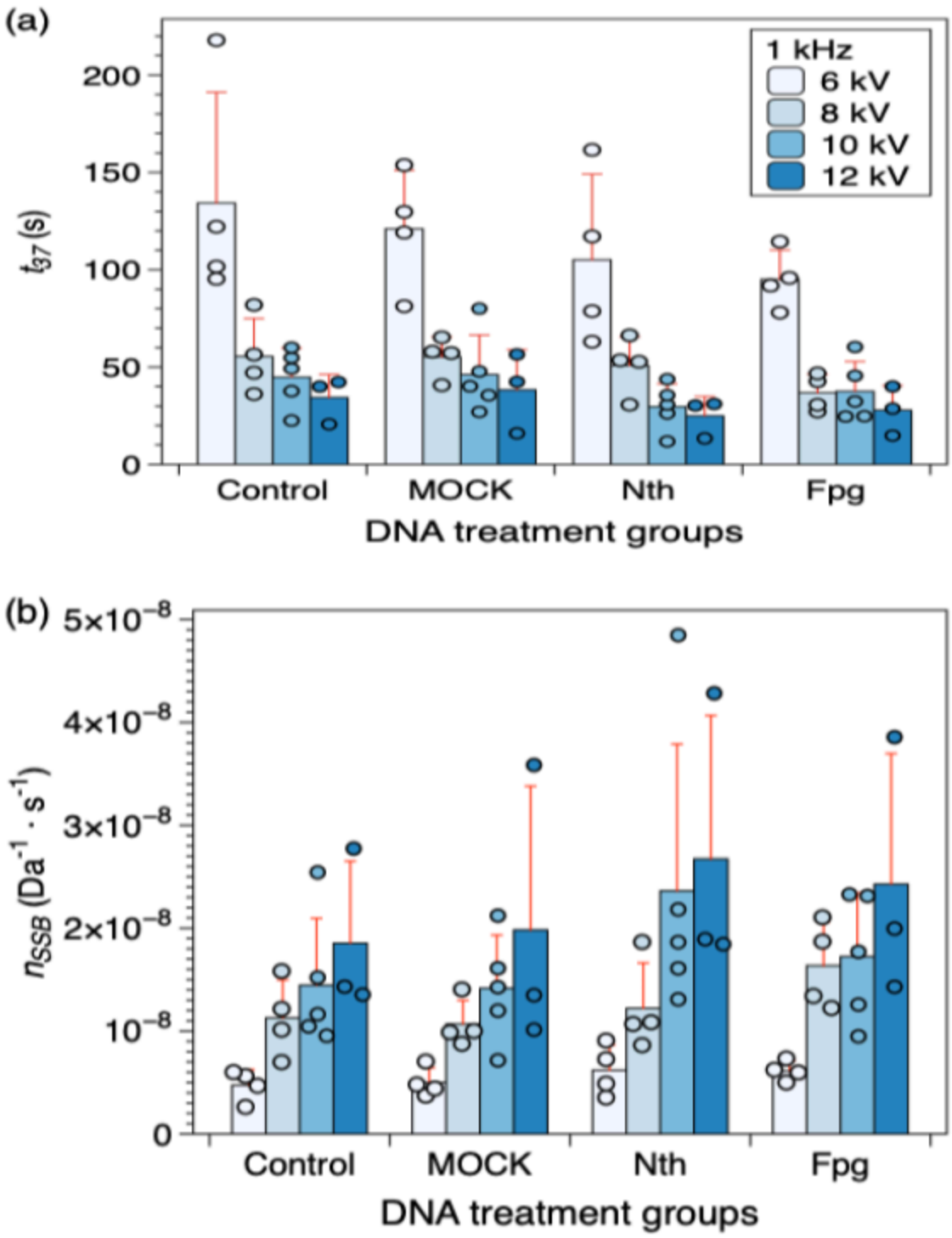

Figure 3

The t_{37} (a) and n_{SSB} (b) values for different treatment groups (Control, MOCK, Nth, and Fpg) at a fixed applied frequency of 1 kHz and applied voltages of 6, 8, 10, and 12 kV. Each point represents the result of an independent experiment, while the bars and associated error bars represent the mean and standard deviation, respectively.

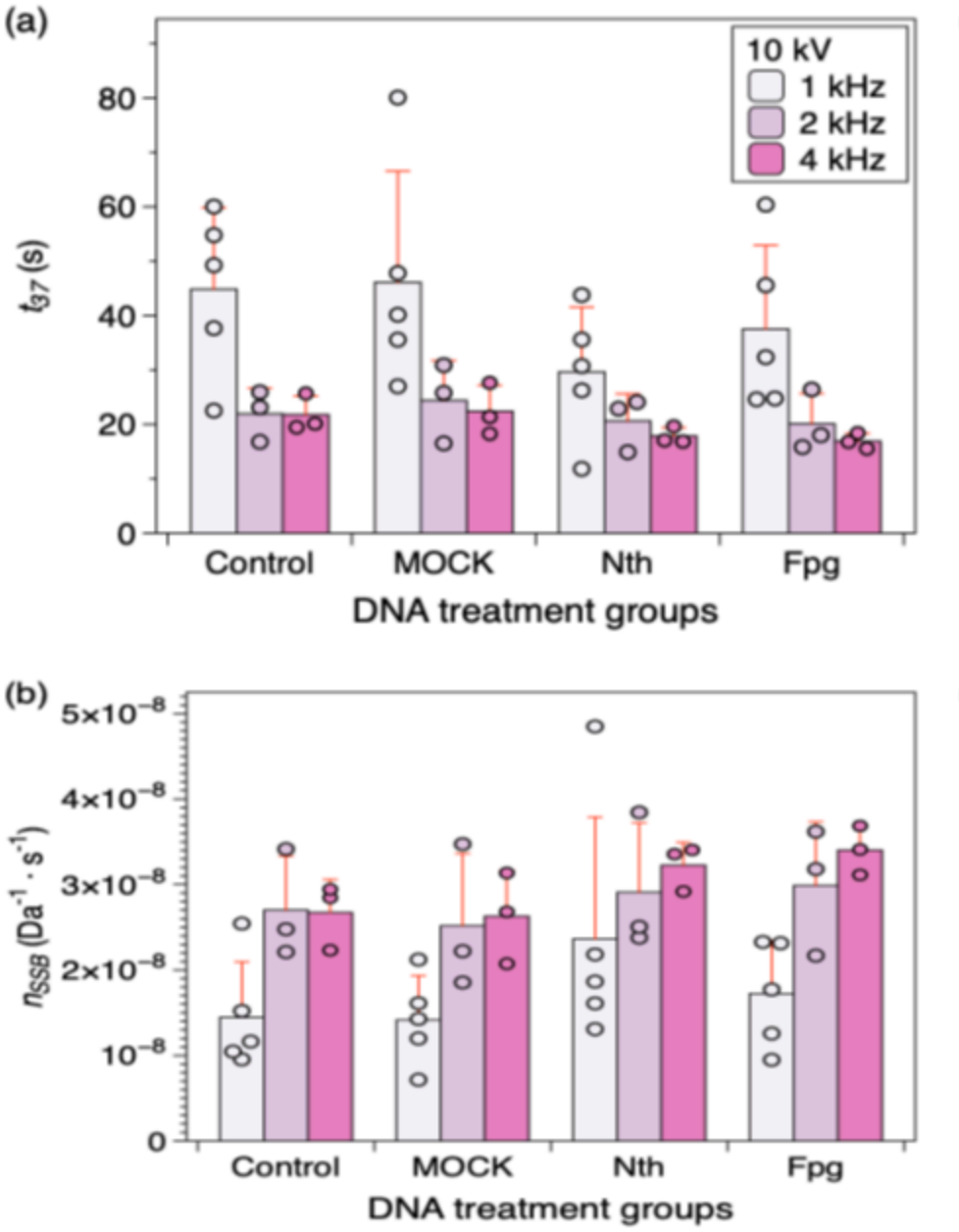

Figure 4

The t_{37} (a) and n_{SSB} (b) values for different treatment groups (Control, MOCK, Nth, and Fpg) at a fixed applied voltage of 10 kV and applied frequencies of 1, 2, and 4 kHz. Each point represents the result of an independent experiment, while the column bars with the associated error bars represent the mean and standard deviation , respectively.

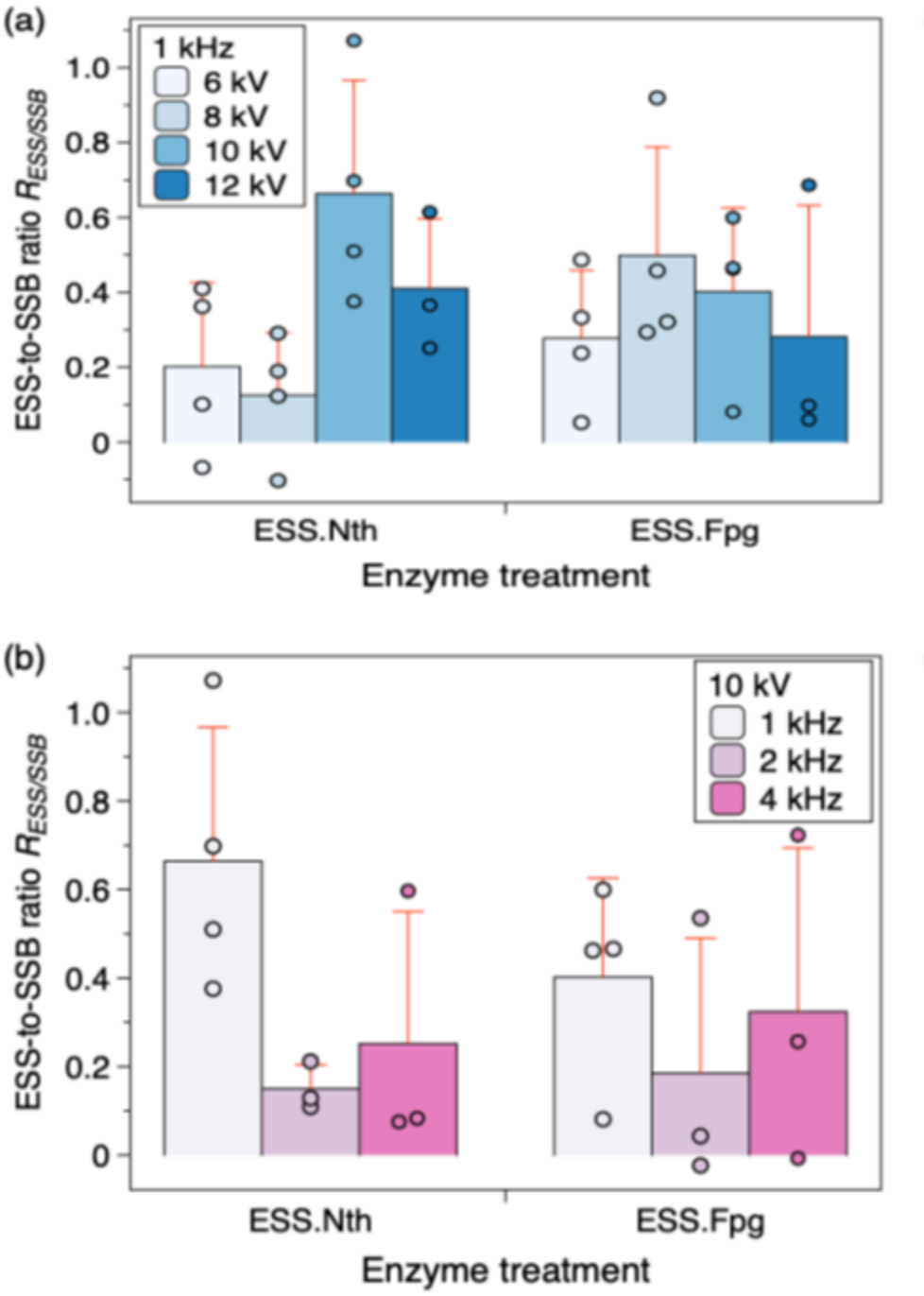

Figure 5

Ratio of ESS to SSB, $RE_{SS/SSB}$, as a function of (a) applied voltage (6, 8, 10, and 12 kV) at a fixed frequency of 1 kHz and (b) applied frequency (1, 2, and 4 kHz) at a fixed voltage of 10 kV.